International Society for Advanced Research

Emerging Technologies, Robotics and Control Systems Volume 1

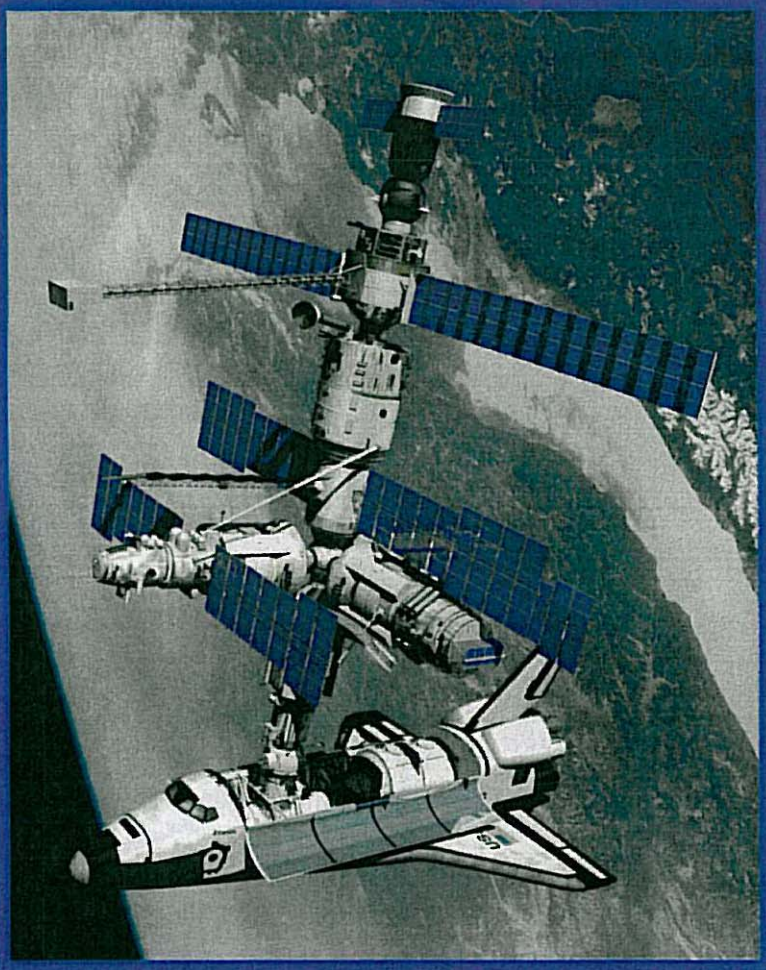

Editor: Salvatore Pennacchio

www.internationalsar.org

Emerging Technologies, Robotics and Control Systems Volume 1

About the book

This book is a collection of papers focused in the field of Emerging Technologies, Control Systems, Robotics and Automation. It presents recent developments and gives the reader a solid background for further studies. The researches presented in this volume have been conducted at the best universities of the world as well as some researches have been conducted at the **NASA** (National Aeronautics and Space Administration) sponsored Structures, Pointing and Control Engineering (SPACE) laboratory.

About the publisher

INTERNATIONALSAR (International Society for Advanced Research) is a new scientific, technical and professional publishing house of books and journals focusing on the wide field of Information Technology.
The main objective of INTERNATIONALSAR is the diffusion of recent research advances in Robotics, Control Systems, Artificial Intelligence, Automation, Telecommunication Systems, Computer Science and Engineering.

€ 90,00

ISBN: 978-88-901928-1-4

On the Sensor Classification Scheme of Robotic Manipulators

Miguel F. M. Lima [1,3], J. A. Tenreiro Machado [2], Manuel Crisóstomo [3], and António Ferrolho [1,3]

[1] *Dept. of Electrical Engineering, School of Technology, Polytechnic Institute of Viseu, Portugal, {lima, antferrolho}@mail.estv.ipv.pt*
[2] *Dept. of Electrical Engineering, Institute of Engineering, Polytechnic Institute of Porto, Portugal, jtm@isep.ipp.pt*
[3] *Instituto de Sistemas e Robotica, Dept. of Electrical and Computer Engineering, University of Coimbra, Portugal, mcris@isr.uc.pt*

Abstract: **This paper analyzes the signals captured during impacts and vibrations of a mechanical manipulator. The Fourier Transform of eighteen different signals are calculated and approximated by trendlines based on a power law formula. A sensor classification scheme based on the frequency spectrum behavior is presented.**

Key-Words: **Vibrations, Impacts, Acquisition System, Robotics, Sensors, Real Time, Fourier Transform**

1. INTRODUCTION

The advent of lightweight arm manipulators, mainly in the aerospace industry, where weight is an important issue, leads to the problem of intense vibrations. On the other hand, robots interacting with the environment often generate impacts that propagate through the mechanical structure and produce vibrations.

In order to analyze these phenomena an acquisition system was developed. The manipulator motion produces vibrations, either from the structural modes or from end-effector impacts. The instrumentation system acquires signals from multiple sensors that capture the joint positions, mass accelerations, forces and moments and electrical currents in the motors. Afterwards, an analysis package, running off-line, reads the data recorded by the acquisition system and extracts the signal characteristics.

Due to the multiplicity of sensors, the data obtained can be redundant because the same type of information could be seen by two or more sensors. Because of the price of the sensors, this aspect can be considered in order to reduce the cost of the system. On the other hand, the placement of the sensors is an important issue in order to obtain the suitable signals of the vibration phenomenon. The study of these issues can help in the design optimization of the acquisition system. In this line of thought a sensor classification scheme is presented.

Several authors have addressed the subject of the sensor classification scheme. White [1] presents a flexible and comprehensive categorizing scheme that is useful for describing and comparing sensors. The author organizes the sensors according to several aspects: measurands, technological aspects, detection means, conversion phenomena, sensor materials and fields of application. Michahelles and Schiele [2] systematize the use of sensor technology. They identified six dimension of sensing that represent the sensing goals for physical interaction.

Today's technology offers a wide variety of sensors. In order to use all the data from the diversity of sensors a framework of integration is needed. There are several techniques used for the sensor fusion when dealing with problem of combing information from several sensors to get a more general picture of a given situation. Examples of fusion methods include weighted decision methods (voting techniques), classical inference, Bayesian inference, Dempster-Shafer's method, fuzzy logic, and neural networks. The study of data fusion has been receiving considerable attention [3] [4]. A survey of sensor fusion for robotics can be found in [5]. Henderson and Shilcrat [6] introduced the concept of *logical sensor*, consisting in a specification for the abstract definition of a sensor that can be used to provide a uniform framework for multisensor system integration.

Latest developments in micro electro mechanical sensors (MEMS) with wireless communication capability make wireless sensor networks possible with promising capabilities. This technology is being proposed for different applications [7], including robotics. In [8] a classification of the wireless sensor network devices is established according to their functionalities and attributes.

This paper is a first step towards the development of a sensor classification scheme based on the frequency spectrum of the signals.

Bearing these ideas in mind, this paper is organized as follows. Section 2 describes briefly the robotic system enhanced with the instrumentation setup. Section 3

presents the experimental results. Finally, section 4 draws the main conclusions and points out future work.

2. Experimental Platform

The developed experimental platform has two main parts: the hardware and the software components. The hardware architecture is shown in figure 2.1. Essentially it is made up of a robot manipulator, a Personal Computer (PC) and an interface electronic system.

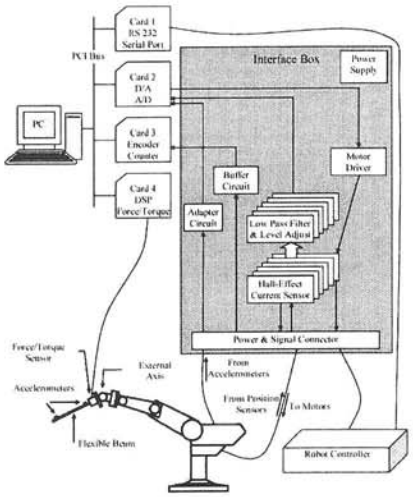

Fig. 2.1 Block diagram of the hardware architecture.

The interface box is inserted between the robot arm and the robot controller, in order to acquire the internal robot signals; nevertheless, the interface captures also external signals, such as those arising from accelerometers and force/torque sensors, and controls the external micro-arm. The modules are made up of electronic cards specifically designed for this work. The function of the modules is to adapt the signals and to isolate galvanically the robot's electronic equipment from the rest of the hardware required by the experiments.

The software package runs in a Pentium 4, 3.0 GHz PC and, from the user's point of view, consists on two applications: (*i*) the acquisition application is a real time program responsible for acquiring and recording the robot signals; (*ii*) the analysis package runs off-line and handles the recorded data.

3. Experimental Results

A steel rod flexible link is used in the experiment. To test the impacts, the link consists on a long, thin, round, flexible steel rod clamped to the end-effector of the manipulator. The robot motion is programmed in a way such that the rod moves against a rigid surface. Figure 3.1 depicts the robot with the flexible link and the impact surface. The physical properties of the flexible beam are shown in Table 3.1.

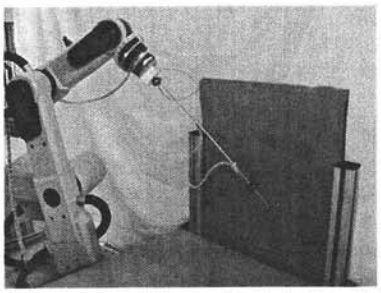

Fig. 3.1 Steel rod impact against a rigid surface.

Table 3.1 Physical properties of the flexible beam.

Characteristics	Thin rod
Material	Steel
Density [kg m^{-3}]	7.86×10^{3}
Elasticity Modulus [N m^{-2}]	200×10^{9}
Mass [kg]	0.107
Length [m]	0.475
Diameter [m]	5.75×10^{-3}

During the motion of the manipulator the clamped rod is moved by the robot against a rigid surface. An impact occurs and several signals are recorded with a sampling frequency of $f_s = 500$ Hz. The signals come from different sensors, such as accelerometers, force and torque sensor, position encoders and current sensors.

In order to have a wide set of signals captured during the impact of the rod against the vertical screen thirteen trajectories were defined. Those trajectories are based on several points selected systematically in the workspace of the robot, located on a virtual Cartesian coordinates system (see figure 3.2). This coordinate system is completely independent from that used on the measurement system. For each trajectory the motion of the robot begins in one of these points, moves against the surface and returns to the initial point. A paraboloid profile was used for the trajectories.

3.1 Time domain

A typical time evolution of the signals is depicted in figures 3.3 to 3.7, corresponding to the cases: (*i*) without impact, (*ii*) the impact of the rod on a gross

screen and (*iii*) the impact of the rod on a thin screen. In this example, the signals present clearly a strong variation at the instant of the impact that occurs, approximately, at $t = 3$ sec. Consequently, the effect of the impact forces and moments, shown on figures 3.3

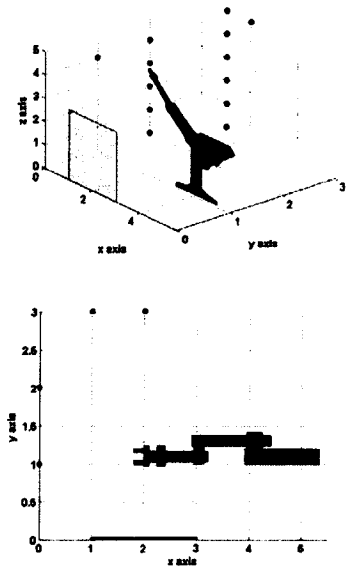

Fig. 3.2 Schematic representation {3D, 2D} of the robot and the impact surface on the virtual cartesian coordinates system.

and 3.4, respectively, is reflected in the current required by the robot motors (Fig. 3.6). Moreover, the amplitudes of forces and torques due to the gross screen (case *ii*) are higher than those corresponding to the thin screen (case *iii*), as would be expected.

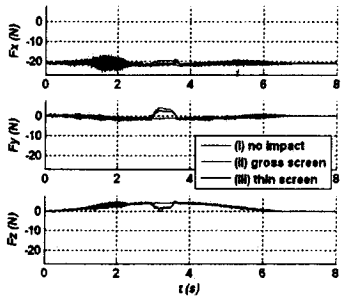

Fig. 3.3 Forces at the gripper sensor.

Figure 3.5 presents the accelerations at the rod free-end (accelerometer 1), where the impact occurs, and at the rod clamped-end (accelerometer 2). The amplitudes of the accelerometers signals are higher near the rod impact side.

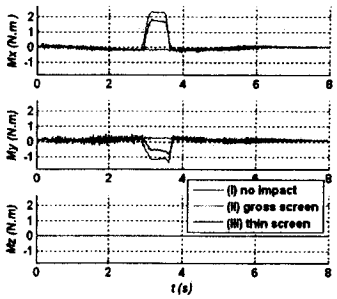

Fig. 3.4 Torques at the gripper sensor.

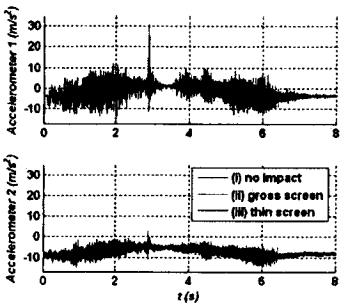

Fig. 3.5 Rod accelerations.

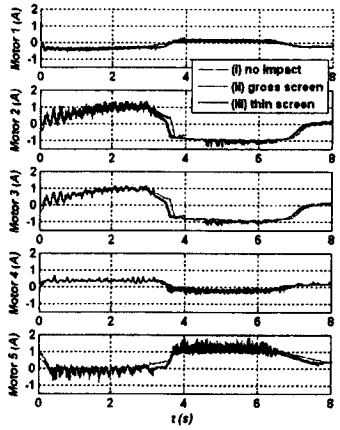

Fig. 3.6 Electrical currents of robot axis motors.

Figure 3.7 shows the five robot axis positions. As mentioned before, for each defined trajectory, the final position is identical to the initial position, as can be seen by the values of position encoders for all axes. The initial values shown for positions are zero because the encoder counters of the measurement system are

reset for each trajectory.

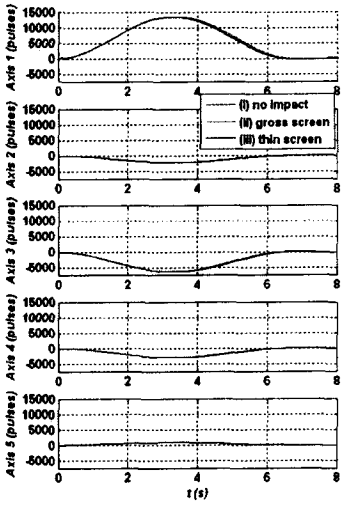

Fig. 3.7 Robot axis positions.

3.2 Frequency domain

Figures 3.8 to 3.13 show, as examples, the amplitude of the Fast Fourier Transform (FFT) of some signals captured during the same impact trajectory. These figures illustrate the different behaviors of the spectrum, depending on the signal in study. All the signals of the trajectories set referred previously were studied, but due to space limitations we are only depicting the most relevant.

In order to examine the behavior of the signal FT, in a systematic way, a trendline was superimposed over the spectrum over, at least, one decade. The trendline is based on a power law approximation [9]:

$$\left|\mathcal{F}\{f(t)\}\right| \approx c\omega^{m}, \qquad (3.1)$$

where $\mathcal{F}$ is the signal FT, $c \in \Re$ is a constant that depends on the amplitude, ω is the frequency and $m \in \Re$ is the slope.

The slope value m of the trendlines is indicated in the figures 3.8-3.12. For each type of signal, the frequency interval was defined approximately in the middle range of the frequency content of the signal.

Figure 3.8 shows the amplitude of the FFT of the axis 3 position signal. A trend line was calculated, and super imposed to the signal (case *iii*). The others position signals were studied, revealing also an identical behavior in terms of its spectrum spread, both under impact and no impact conditions. The spectrum was approximated by trendlines in a frequency range larger than one decade.

Figure 3.9 shows the amplitude of the FFT of the electrical current for the motor axis 3 (case *ii*). The spectrum was also approximated by a trendline in a frequency range larger than a decade.

According to the robot manufacturer specifications the loop control of the robot has a cycle time of $t_c = 10$ ms. This fact is observed approximately at the fundamental ($f_c = 100$ Hz) and multiple harmonics in all spectra of motor currents.

Figure 3.10 shows the amplitude of the FFT of the F_z force (case *i*). This spectrum is not so well defined in a large frequency range. Nevertheless, the spectrum was approximated by a trendline in a frequency range of approximately one decade in order to get a systematic method of comparison.

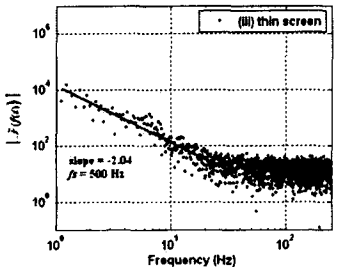

Fig. 3.8 Spectrum of the axis 3 position.

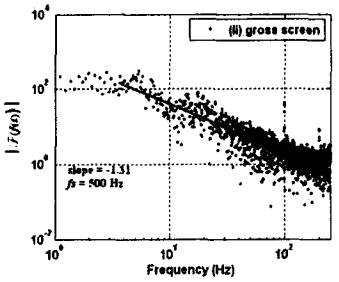

Fig. 3.9 Spectrum of the axis 3 motor current.

Figure 3.11 shows the amplitude of the FFT of the M_z torque (case *i*). As for F_z force shown before, this spectrum is not so well defined in a large frequency range. The spectrum was approximated by a trendline in a frequency range of approximately one decade.

Finally, Fig. 3.12 depicts the spectrum of the signal captured from the accelerometer 2 (case *i*) located at the rod clamped-end of the beam. The spectrum was approximated by a trendline in a frequency range of

approximately one decade.

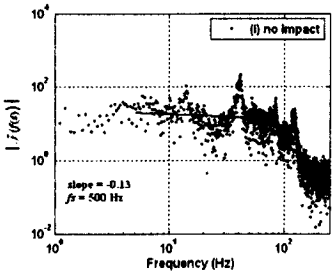

Fig. 3.10 F_z force spectrum.

Figure 3.13 shows the amplitude *versus* phase of the F_z force spectrum (case *i*). There is a large dispersion of the phase. Therefore the phase is not suitable for comparing the spectrum behavior.

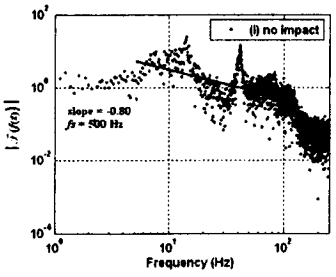

Fig. 3.11 M_z torque spectrum.

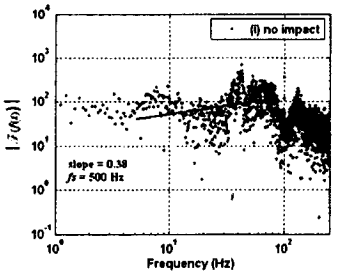

Fig. 3.12 Acceleration spectrum of the rod clamped-end.

While the trendlines used for the electrical currents and position signals FT seem appropriate, the same technique used for the forces/moments and acceleration signals is questionable. However, in spite of this, trendlines were used for all FT signals in order to obtain comparable units. In fact, we are trying to establish a relationship between signals of the same system based on the spectrum behavior. There are others approaches as, for example, the correlation between the signals that is currently under development.

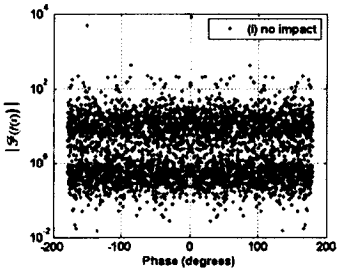

Fig. 3.13 Amplitude *versus* phase of the F_z force spectrum.

3.3 Spectrum trendlines slopes analysis

Based on the several values of the spectrum trendlines slopes some statistics can be performed. During each trajectory of the robot eighteen signals were captured. For each trajectory there are three cases: (*i*) without impact, (*ii*) the impact of the rod on a gross screen and (*iii*) the impact of the rod on a thin screen. As referred before, thirteen trajectories were defined. These samples lead to a population of 702 slope values.

A box plot provides a visual summary of many important aspects of data distribution. It indicates the median, upper and lower quartile, upper and lower adjacent values (whiskers), and the outlier individual points. The interpretation of the boxplot (see figure 3.14) is as follows. The line inside the box shows the median (middle point value) of the data. The box is drawn so that 50% of the data will reside inside the box. Also, 75% of the data has values smaller than the top of the box and 25% of the data have values smaller than the bottom of the box. The top and bottom lines are the whiskers that extend from the box to show the range of the data. Outliers points (extreme values) are plotted as individual plus (+) symbol outside the whiskers.

Figure 3.14 shows the statistics of the spectrum trendlines slopes for the gross screen (case *ii*). Figure 3.15 shows the statistics of the spectrum trendlines slopes for all the cases: (*i*) without impact, (*ii*) the impact of the rod on a gross screen and (*iii*) the impact of the rod on a thin screen.

Finally, figure 3.16 depicts the interquartile range (IQR) *versus* the median. The IQR is obtained by subtracting the lower (first) quartile value from the upper (third) quartile value. The IQR is a robust way of describing the dispersion of the data. From figure 3.16 we can define three groups of signals. The

ellipses depicted in the chart represent these groups. The forces $\{F_x, F_y, F_z\}$ and the accelerations $\{A_1, A_2\}$ signals are closed. Positions $\{P_1, P_2, P_3, P_4, P_5\}$, moments $\{M_x, M_y\}$ and I_3 signals are located on the left side of the figure 3.16. Finally, electrical currents $\{I_1, I_2, I_4, I_5\}$ are situated in the middle of the chart and near each other. It rests the M_z signal that apparently is alone. A deeper insight into the nature of this feature must be envisaged to understand the behavior of the I_3 and M_z signals. Comparing figures 3.14 and 3.15, it can be seen that the spectrum is basically the same for the case of the impact against a gross screen and for the other cases.

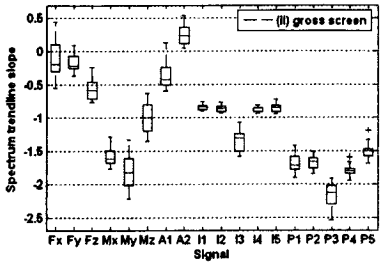

Fig. 3.14 Statistics of spectrum trendlines slopes for the gross screen.

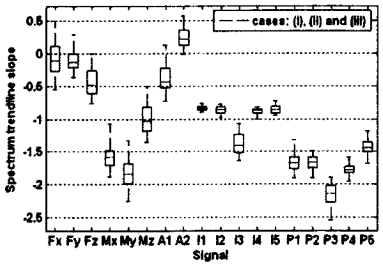

Fig. 3.15 Statistics of spectrum trendlines slopes for all the cases (*i, ii, iii*).

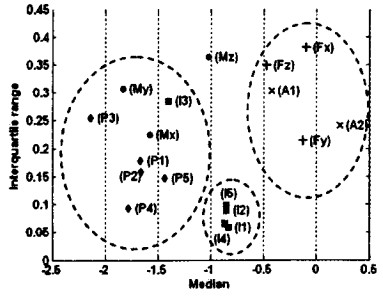

Fig. 3.16 IQR *versus* median for all the cases (*i, ii, iii*).

4. Conclusion

In this paper an experimental study was conducted to investigate several robot signals both under impact and no impact conditions. It was shown that the spectrum was basically the same for the case of the impact against a gross screen and for the other cases. A sensor classification scheme was presented. The adopted methodology leads to arrange the robotic signals in terms of identical spectrum behavior, obtaining three groups of signals. This observation merits a deeper investigation as it gives rise to new valuable results to instrument control applications.

In future work, we plan to pursue several research directions to help us further understand the behavior of the signals. These include the use of different rods for impact and others techniques to measure the similarities of the signals.

References

[1] R. M. White. A sensor classification scheme. *IEEE Trans. on Ultrasonics, Ferroelectrics and Frequency Control*, 34(2):124–126, 1987.

[2] F. Michahelles and B. Schiele. Sensing opportunities for physical interaction. *Workshop on Physical Interaction (PI03) at Mobile HCI*, Udine, Italy, 2003.

[3] R. C. Luo and M. G. Kay. A tutorial on multisensor integration and fusion. In *IEEE 16th Annual Conf. of Industrial Electronics Society*, pages 707–722, 1990.

[4] Jaime Esteban, Andrew Starr, Robert Willetts, Paul Hannah, and Peter Bryanston-Cross. A review of data fusion models and architectures: towards engineering guidelines. *Neural Computing & Applications*, 14(4):273–281, 2005.

[5] J. K. Hackett and M. Shah. Multi-sensor fusion: a perspective. In *Proc. IEEE Int. Conf. on Robotics & Automation*, pages 1324–1330, 1990.

[6] Henderson, T. C., and E. Shilcrat, Logical sensor systems. *J. of Robotic Systems*, vol. 1, no. 2, pp. 169-193, 1984.

[7] Arampatzis, Th Lygeros, J. Manesis, S., A Survey of Applications of Wireless Sensors and Wireless Sensor Networks, *Proc. IEEE Int. Symp. on Intelligent Control*, pp. 719-724, 2005.

[8] S. Cheekiralla, D.W. Engels, A functional taxonomy of wireless sensor network devices, Auto ID Laboratory, MIT, Cambridge, USA.

[9] Miguel F. M. Lima, J. A. Tenreiro Machado, Manuel Crisóstomo, Windowed Fourier transform of experimental robotic signals with fractional behavior, In *Proc. IEEE Int. Conf. on Computational Cybernetics*, August, 2006, Tallin, Estonia.